A Synthetic Acetyl-CoA Bi-cycle Synergizes the Wood-Ljungdahl Pathway for Efficient Carbon Conversion in Syngas Fermentation

Chao Wu
National Renewable Energy Laboratory
Jonathan Lo
National Renewable Energy Laboratory
Chris Urban
National Renewable Energy Laboratory
Xiang Gao
National Renewable Energy Laboratory
Jonathan Humphreys
National Renewable Energy Laboratory
Shrameeta Shinde
Miami University
Xin Wang
Miami University https://orcid.org/0000-0002-7174-3042
Katherine Chou
National Renewable Energy Laboratory
PinChing Maness
National Renewable Energy Laboratory
Nicolas Tsesmetzis
Shell International Exploration and Production Inc. https://orcid.org/0000-0001-5246-0568
David Parker
Shell International Exploration and Production Inc
Wei Xiong (Wei.Xiong@nrel.gov)
National Renewable Energy Laboratory

Article

Keywords: synthetic acetyl-CoA bi-cycle, Wood-Ljungdahl pathway (WLP), carbon conversion, syngas fermentation

Posted Date: October 13th, 2020

DOI: https://doi.org/10.21203/rs.3.rs-85001/v1

A Synthetic Acetyl-CoA Bi-cycle Synergizes the Wood-Ljungdahl Pathway for Efficient Carbon Conversion in Syngas Fermentation

Chao Wu[a]†, Jonathan Lo[a]†, Chris Urban[a], Xiang Gao[a], Jonathan Humphreys[a], Shrameeta Shinde[b], Xin Wang[b], Katherine J. Chou[a], PinChing Maness[a], Nicolas Tsesmetzis[c], David Parker[c], Wei Xiong[a]*

[a] Biosciences Center, National Renewable Energy Laboratory, Golden, CO 80401, USA

[b] Department of Microbiology, Miami University, Oxford, OH 45056, USA

[c] Shell International Exploration and Production Inc, Houston, TX 77082, USA

* Correspondence to: Wei.Xiong@nrel.gov

† Denotes equal contribution

Abstract

The Wood-Ljungdahl pathway (WLP) is a natural carbon fixation pathway capable of converting one-carbon (C1) compounds (CO_2, CO, formate) to two-carbon (C2) metabolite acetyl-CoA or coordinating with canonical glycolysis to convert sugar feedstocks to acetyl-CoA with high carbon yield. The catalytic inefficiency and engineering difficulty in key enzymes, however, limit the biosynthetic potential of this pathway. Here we design a synthetic acetyl-CoA bi-cycle to synergize the WLP for efficient C2 metabolite synthesis. This pathway produces an acetyl-CoA by fixation of two CO_2 equivalents *via* three functional modules acting in series: carbon fixation, gluconeogenesis, and non-oxidative glycolysis. We examine the pathway through comprehensive *in silico* thermodynamic and kinetic analyses. The prototypic pathway is implemented in a syngas-fermenting *Clostridium ljungdahlii* DSM 13528 by expressing a heterologous phosphoketolase and coordinating with native enzymes in the host acetogen. We demonstrated the effectiveness of this synthetic pathway in carbon conversion under various growth conditions, which complements the WLP for valorization of syngas as well as sugar feedstocks with high catalytic efficiency. This study underscores the reductive acetyl-CoA bi-cycle as a practical strategy to improve carbon conversion and redox homeostasis in the acetogenic host.

Introduction

Syngas, a gas mixture consisting of carbon monoxide (CO), hydrogen (H_2), and carbon dioxide (CO_2) can be converted and upgraded by anaerobic acetogens[1]. As a standalone bioprocess or coupled with sugar conversion mixotrophically[2], syngas fermentation provides an attractive strategy to valorize low-cost substrates, waste streams, and produce fuels as well as value-added chemicals. Compared to thermochemical processes, biological syngas conversion has numerous advantages including: a higher tolerance to impurities such as sulfur compounds in syngas, a wider range of usable H_2, CO_2, and CO mixtures, a lower operating-temperature and -pressure, and higher product yield and uniformity[3]. However, broad use of this bioprocess needs to overcome technical bottlenecks such as fundamental limits in cell metabolism and enzyme kinetics that could lead to catalytic inefficiency.

Syngas-fermenting bacteria utilize the Wood-Ljungdahl pathway (WLP), converting CO_2/CO to acetyl coenzyme A (CoA), the key precursor of biomass components and fermentation products (acetate, ethanol, butanol, *etc.*). This carbon fixation pathway synthesizes acetyl-CoA (C2) through a CO-methylating acetyl-CoA synthase (ACS), which combines CO (C1) with CoA and a methyl group (C1, initially from CO_2) to realize "**C1 + C1 = C2**". The apparent simplicity of this linear pathway, however, relies on the complex, interconnected enzymatic mechanisms that enable carbon fixation. ACS, for example, consists of three functionally diverse subunits that associate tightly in a complex with carbon monoxide dehydrogenase (CODH), and utilizes the product of the CODH reaction (CO) as its substrate in a kinetically coupled reaction linked to the generation of acetyl-CoA[4]. The complexity of the native C1/C2 biochemistry renders enzyme modification and pathway engineering a grand challenge. In addition, the WLP was identified with rate-limiting steps including formation of 10-formyl-tetrohydrofolate, a key intermediate in the methyl branch by the synthetase which occurs with a very low k_{cat} value (1.4 s^{-1} for the enzyme from *Moorella thermoacetica*)[5]. To optimize syngas bioconversion, an engineering-amenable pathway with enzymes of superior catalytic

kinetics is pursued. However, beyond the WLP, no such a natural pathway was found so far in syngas-fermenting bacteria capable of converting C1 compounds to acetyl-CoA.

In recent years, synthetic pathways have been proposed to reduce carbon loss during acetyl-CoA synthesis, including a non-oxidative glycolysis (NOG)[6] that can bypass the C3 decarboxylation step in the canonical glycolytic pathway. The NOG pathway converts two glyceraldehyde 3-phosphate (C3) into three molecules of acetyl-phosphate (C2) without carbon loss. Other carbon conservation solutions entail the use of native carbon-fixing pathways, for example, reversed pyruvate:ferredoxin oxidoreductase (rPFOR) which is evolved in anaerobes for CO_2 incorporation by converting acetyl-CoA to pyruvate (C3) [8]. However, whether and how these pathways could apply to syngas-fermenting bacteria for augmenting carbon fixation efficiency remain elusive.

Here we introduce a synthetic acetyl-CoA bi-cycle to circument the suboptimality of the WLP in C2 metabolites synthesis. The bicyclic pathway aims to synthesize an acetyl-CoA by fixation of two CO_2 equivalents and to maximize the use of native enzymes in the host's metabolism. We first investigate the feasibility of the acetyl-CoA bi-cycle *in silico* and validate the functionality of essential pathway modules in a model syngas-fermenting chassis *Clostridium ljungdahlii*[7]. As a proof-of-concept, we engineer the prototypic acetyl-CoA bi-cycle in the bacteria and demonstrate the beneficial effects of coupling the bi-cycle with the WLP for efficient C2 metabolites synthesis.

Results

Design of the bicyclic acetyl-CoA pathway for syngas-fermenting bacteria

Rational combination of the carbon-neutral metabolism and CO_2 fixation enzyme leads to a new pathway for acetyl-CoA synthesis. We term it as reductive acetyl-CoA bi-cycle. As illustrated in Fig.1a and detailed in Fig.1b, this pathway consists of three functional modules: 1. Carbon fixation *via* rPFOR to realize C1 + C2 = C3 (CO_2 + Acetyl-CoA = Pyruvate); 2. Gluconeogenesis module to convert two pyruvate generated in Module 1 to one hexose phosphate: C3 + C3 = C6 (2 Pyruvate = Hexose); 3. NOG module which converts one hexose sugar to three acetyl-CoA: C6 = 3 × C2 (Hexose = 3 × Acetyl-CoA). Two of three generated acetyl-CoA can replenish the initial investment of the C2 metabolite. In terms of net stoichiometry, this pathway realizes C1 + C1= C2 (CO_2 + CO_2

= Acetyl-CoA) while bypassing ACS/CODH complex and other rate-limiting enzymes in the WLP. The key carbon-fixing enzyme in the pathway is rPFOR, which is native in many syngas-fermenting bacteria and can operate in the reductive direction[8, 9]. Besides PFOR, the pathway contains 16 metabolic enzymes, 15 of which are native in acetogens as being found in *C. ljungdahlii* (Table S1). Coupled with a heterologous phosphoketolase that activates the NOG by converting sugar phosphates to acetyl phosphate (C2), the prototype of this bicyclic pathway may be built *in vivo* with minimal genetic modification of the host. In terms of energetic cost, the pathway can use reduced ferredoxin for CO_2 fixation *via* rPFOR. Gluconeogenesis consumes NAD(P)H, and burns ATP to overcome thermodynamic barrier over the conversion of pyruvate to phosphoenolpyruvate. Considering that gluconeogenesis is a native metabolic pathway and functions indispensably in homoacetogens for sugar synthesis from acetyl-CoA, no extra energetic expense will be exerted to the host when incorporating it into the bi-cycle. Acetogens can generate cellular reductants and ATP from syngas and various organic substrates. In a highly reductive syngas ambiance, acetogens produce reducing equivalents directly from H_2 and CO through H_2-uptake hydrogenase and CODH, respectively. Versatile phosphorylation mechanisms including an Rnf complex, a membrane ferredoxin: NAD oxidoreductase in *C. ljungdahlii*, contributes to H^+-translocating ATP synthesis, hence balancing energetic demand[10].

To expand substrate spectrum, functional variants of reductive acetyl-CoA bi-cycle are also designable. For instance, replacing rPFOR by a reversible pyruvate formate lyase (PFL), which is also native in *C. ljungdahlii*, could enable acetyl-CoA synthesis from formate (Fig.1b). In addition, conversion of methanol to acetyl-CoA could be feasible by incorporating two native enzymes in many acetogens: alcohol dehydrogenase (ADH) and aldehyde oxidoreductase (AOR)[11] that convert methanol to formate *via* formaldehyde.

Catalytic properties of the acetyl-CoA bi-cycle

Evaluating pathway properties for massive possible physiological scenarios is computationally feasible. We therefore examine the designed pathway *in silico* to understand its feasibility. We first modeled the Max-min driving force (MDF)[12, 13] and sought to understand the pathway in a thermodynamic landscape. Even though this

pathway has reversible reactions such as PFOR which could have high activity toward oxidative direction, optimization of metabolite concentrations in a physiological range enables all reactions thermodynamically favorable ($\Delta G' < 0$). It indicates that the thermodynamic driving force can effectively drive the pathway toward the formation of acetyl-CoA (Fig.2). To evaluate the catalytic property of this pathway, we performed enzymatic protein cost analysis[12, 14] which takes both reaction thermodynamics and enzyme kinetics into account and calculates the theoretical lower bound of protein expense that affords the production of an acetyl-CoA unit. Interestingly, despite more reactions than in the WLP, the bi-cycle expends much lower protein cost than the WLP (1.5×10^4 g/(mol s^{-1}) vs. 9.4×10^4 g/(mol s^{-1})). This result highlights superior catalytic efficiency of the bicyclic pathway.

In addition, we used ensemble modeling to assess metabolic robustness[15, 16], which investigates a set of models with different kinetic parameters and perturbs them by varying maximum rate (V_{max}), which is largely proportional to the expression levels of the enzyme[14, 17]. The synthetic pathway displays a high system stability when overexpressing every pathway enzyme individually by 10-fold, which only leads to less than 20% failure probability (Fig.3a). A moderate robustness is also exhibited when pathway enzymes are downregulated. In 15 of 18 enzymes, greater than 50% probability of success can still be achieved when knocking them down by an order of magnitude. Pathway stability is sensitive to the downregulation of phosphoketolase (pkt), fructose-1,6-bisphosphatase (fbp), and phosphoenolpyruvate carboxykinase (pepck) as the perturbation might drain their reaction products, which are the substrates of the next reaction, hence forming a kinetic trap. Complementing to robustness analysis, we also investigated the response of metabolic flux to perturbed enzyme level and showed that the pathway flux is tunable by altering certain enzyme expression levels (Fig.3b). For example, overexpression of pepck and fbp by 10-fold tends to change pathway fluxes by 1.5-fold, indicating there exist operable rate-determining steps in the pathway for flux control.

Next, we evaluated the biosynthetic potential of the acetyl-CoA bi-cycle in the context of metabolic network by using a genome-scale model for flux balance analysis (FBA)[18, 19]. *C. ljungdahlii* genome carries all genes in the acetyl-CoA bi-cycle except the phosphoketolase gene. We thus added this reaction into the stoichiometric model and

tested maximal carbon yield (represented as the flux for ethanol and acetate production) as a function of the acetyl-CoA bi-cycle (represented by phosphoketolase flux) and the WLP (represented by ACS flux) (Fig.4). When fructose serves as the sole carbon source in heterotrophic mode, we observed a coordination of synthetic acetyl-CoA bi-cycle and native WLP to raise carbon yield of the C2 metabolites (Fig. 4b). Synergetic improvement is also observed when fructose and CO are provided in mixotrophic mode, indicating a potential impact of the bi-cycle to improve carbon efficiency under this feeding condition (Fig. 4c). With a mixture of CO, CO_2 and H_2, the implementation of the bi-cycle appears to improve the carbon yield again (Fig.4a), when phosphoketolase flux is ranged between 0-10 mmol $gDCW^{-1}$ h^{-1}. Note that a tightly constrained FBA model is used where the production and consumption of redox cofactors (*e.g.* ferredoxin and NAD(P)H) must be balanced. Under this reductive limitation in cellular level, the bi-cycle appears to improve the fluxes for C2 metabolites (acetate and ethanol) production, implying its potential value in metabolic engineering of acetogens.

C. ljungdahlii carries functional modules of the acetyl-CoA bi-cycle

Prior to engineering a prototypic acetyl-CoA bi-cycle in *C. ljungdahlii,* we first examined the activities of the native carbon fixation module and the gluconeogenesis module since these genes are present in the *C. ljungdahlii* genome. We designed an isotope labeling experiment in which ^{13}C-acetate (^{13}C in place for both methyl and carboxyl carbons) was used as a tracer and the ^{13}C-fingerprints of target metabolites were recorded (Fig.5). When CO/CO_2 (4:1) was provided in the headspace of clostridial culture, ^{13}C-acetate was assimilated into the central carbon metabolism (CCM) *via* activated forms, *e.g.,* acetyl-CoA or acetyl phosphate. Their bioconversion was further tracked by positional ^{13}C-patterns of proteinogenic amino acids that are produced from the CCM. Specifically, two carbon (C2-3) labeled alanine was observed. This labeling pattern is in line with the activity of carbon fixation module in which rPFOR incorporates a ^{13}C-acetyl-CoA with an unlabeled CO_2 for the synthesis of pyruvate, the precursor of alanine. In addition, ^{13}C-pyruvate propagated its labeled carbons to oxaloacetate (OAA) which was reflected by ^{13}C-pattern of aspartate consistently. The conversion of OAA to PEP was also detected by the labeling of PEP in the corresponding positions (PEP2-3), consistent with the

activity of PEP carboxykinase, a key reaction in gluconeogenesis. Moreover, we also detected ^{13}C-labeling on corresponding positions in histidine and tyrosine. These two amino acids are synthesized from sugar phosphates (erythrose-4-phosphate and pentose 5-phosphate, respectively). The observed labeling indicates that *C. ljungdahlii* has a complete suite of enzymes to support gluconeogenesis in the conversion of C2 metabolites to sugar phosphates. The activities of separate modules were also examined under heterotrophic condition (Fig.S3) when clostridial cells grew on fructose. Interestingly, we detected the carbon fixation activity by rPFOR but no equivalent gluconeogenesis activity, suggesting that the gluconeogenesis module is optional when cells are supplied with sufficient sugar substrates.

Overexpression of heterologous phosphoketolase enabled a complete acetyl-CoA bi-cycle in the host

We further expressed a heterologous phosphoketolase in *C. ljungdahlii* to enable a NOG module and complete the acetyl-CoA bi-cycle. We selected a phosphoketolase gene from *C. acetobutylicum* and tested its enzymatic activity by expressing it in *E. coli,* followed by enzyme purification and in vitro assay (Fig.S4). The gene was then cloned into a plasmid (pMTL82151) where the sequence is placed behind the non-coding sequence harboring the native promoter for *pta* gene (encoding phosphotransacetylase) and the plasmid was transformed into wild type *C. ljungdahlii*. The activity of phosphoketolase in cell lysate was determined to be 1.12 ± 0.08 μmol min^{-1} mg^{-1}. We further performed quantitative proteomic analysis of the new strain (named as *acb*, standing for Acetyl-CoA Bi-cycle) that was constructed. All enzymes essential in the bi-cycle including heterologously expressed phosphoketolase were detected in the proteome, accounting for 8.7% of metabolism proteome (Fig.6). As a comparison, enzymatic proteins for the WL pathway account for 24.2% of the proteome in metabolism category. These results indicated the acb strain expressed all enzymes in the acetyl-CoA bi-cycle and can serve as a prototype cell model for investigating this synthetic pathway.

The acetyl-CoA bi-cycle improved carbon utilization efficiency and/or redox homeostasis in *C. ljungdahlii*

We thus examined the growth and productivity of the acb strain under various growth conditions. The acb strain exhibited 20% higher heterotrophic growth rate than the wild type ($4.9\times10^{-2} \pm 3.4\times10^{-3}$ vs. $4.0\times10^{-2} \pm 2.8\times10^{-4}$) when fructose was supplied as the carbon source (Fig. 7b). Correspondingly the fructose consumption rate, acetate, and ethanol production rate of the acb strain increased by 31%, 24%, 52%, respectively, compared to the parental strain (Fig.7b). These results indicate that heterologously expressed phosphoketolase improved sugar conversion rate in *C. ljungdahlii*. We then investigated the impact of this genetic engineering on carbon conversion efficiency. The acb strain exhibited 84% carbon molar yield for converting fructose to acetate and ethanol, comparable to the value in wild type *C. ljungdahlii* (86%, Fig.S6) and exceeding theoretical maximum of the canonical glycolytic pathway (67%). To distinguish the contribution of NOG and WLP, both of which increase carbon yield over glycolysis, we utilized a *WLP-* mutant and transformed the pMTL82151 plasmid carrying phosphoketolase into it. This strain (*Δacs*) has a site-directed mutagenesis in the ACS which leads to inactivation of this key WLP enzyme. Deficient ACS lowered the carbon molar yield from 86% (as in WT) to nearly 71% in *Δacs*, consistent with the role of WLP in improving heterotrophic carbon yield. We then investigated the effect of heterologous phosphoketolase expression in *Δacs* background strain (named as acb*Δacs*). We observed no obvious increase in carbon yield but interestingly, significant improvement of ethanol to acetate ratio (1.60 ± 0.04 vs. 0.80 ± 0.09, Fig.S7). Since ethanol is a more reduced C2 product than acetate, we hypothesize that this is an outcome of redox homeostasis in *Δacs,* and the NOG module elevates the proportion of reduced product as a trade-off of total carbon yield. To test this hypothesis, we leveraged a genome scale *C. ljungdahlii* FBA model with ACS knocked out, phosphoketolase knocked in, and all redox reactions balanced. Indeed, ethanol/acetate ratio is monotonically increasing with phosphoketolase flux, given a certain production rate for ethanol and acetate (represented by contour in Fig.S8). Our experimental results as well as *in silico* analysis demonstrate a new role of the NOG module in improving sugar conversion rate and redox homeostasis.

We next tested the performance of acetyl-CoA bi-cycle under mixotrophic conditions. The acb strain exhibited 21% higher mixotrophic growth rate than the wild type ($2.3\times10^{-2} \pm$

4.8×10^{-4} vs. $1.9\times10^{-2} \pm 2.5\times10^{-3}$) when fructose and gaseous substrates (CO/CO_2) were available in the culture system (Fig.7c). Consistently the rates for consuming fructose and producing C2 products (acetate and ethanol) increased by 56%, 39%, respectively. The headspace pressure also decreased more quickly than the control culture, indicating a faster consumption rate of gaseous substrates.

Without fructose supplied, both acb and wild type strains can grow autotrophically using CO and CO_2 as the carbon sources. Under this condition, the acb strain displayed similar C2 production rate (acetate and ethanol) with the parental strain while the ethanol to acetate molar ratio is lower (1.2 ± 0.2 vs. 1.7 ± 0.2). This result is likely consistent with the global redox balancing required in anaerobic cells, as more electrons are consumed for CO_2 fixation in acetyl-CoA bi-cycle than the WLP. Nevertheless, the acb strain grew much faster than the wild type *C. ljungdahlii* (specific growth rate: $2.4\times10^{-2} \pm 5.8\times10^{-4}$ vs. $1.4\times10^{-2} \pm 4.4\times10^{-4}$, Fig.7a), indicating that acetyl-CoA bi-cycle in addition to WLP helped chemolithotrophic growth of the cells incrementally. Collectively, our results demonstrated beneficial effect of acetyl-CoA bi-cycle in the host of syngas-fermenting bacteria under various growth modes.

Discussion

Traditional metabolic engineering strategies to improve a metabolic pathway mainly focus on engineering the pathway components directly. However, this approach could be challenging for WLP due to the inherent engineering difficulty on the key pathway enzymes. To our knowledge, no engineering work that has successfully improved the WLP was reported. Here we sought to complement the WLP by constructing a synthetic pathway. The acetyl-CoA bi-cycle provides syngas-fermenting acetogen a new option for carbon conservation/fixation. The acetyl-CoA bi-cycle leverages native enzymes to the largest extent. It does not compete with the major existing metabolic pathways, thus has minimal compatibility issue. Although other CO_2-fixing pathways are available for engineering purpose, it could be more difficult to implement in syngas-fermenting bacteria. The hydroxypropionate/hydroxybutyrate cycle, for example, is reported to synthesize acetyl-CoA from CO_2 equivalents[20]. Sixteen enzymes are required to achieve the complete cycle and most of their genes are not found in syngas-fermenting bacteria.

Their compatibility with the host's metabolic system is uncertain. The canonical Calvin-Benson-Bassham (CBB) cycle is another option. However, the CBB cycle synthesizes triose (C3) not the acetyl-CoA (C2) as the final product. Additional step converting C3 to C2 will lead to carbon loss.

In terms of net stoichiometry of carbon fixation, the acetyl-CoA bi-cycle consumes more ATP and reducing equivalents than the WLP. The bi-cycle might seem a luxurious pathway as three ATP and eight electrons are required for generating an acetyl-CoA from CO_2. Nevertheless, the acetyl-CoA bi-cycle is closely coupled with the CCM, the intermediates from which provides numerous essential precursors to support biosynthesis and cell growth. More importantly, we consider that the design of a synthetic metabolism may not only reflect the energy cost in the pathway but also the amount of enzymatic protein required to sustain pathway flux. We used state-of-the-art computational methods for analyzing pathways in terms of thermodynamics and kinetics and showed that the bi-cycle requires 6-fold less enzymatic protein to achieve the same acetyl-CoA conversion rate as the WLP (Fig.2). Given that enzyme synthesis, assembly and maintenance are among the most expensive chemical processes in a living cell, recruiting acetyl-CoA bi-cycle in synergy with the WLP will endow host cells with additional plasticity to rationalize the allocation of energetic currencies between protein and metabolite level. The acetyl-CoA bi-cycle thus lays a foundation to foster global acetogenic metabolism, while it highlights protein cost as a critical criterion for pathway design.

In addition to protein cost, this study collectively illustrates the bicyclic pathway in terms of thermodynamic feasibility, metabolic stability, biosynthetic potential within a genome-scale metabolic network, *in vivo* module functionalities and actual improvement on acetogenesis. Based on all these results, we posit that coupling the acetyl-CoA bi-cycle with the native WLP is a practical strategy to improve carbon conversion in acetogenic organisms.

Materials and Methods

In silico analysis All computational methods and resources are available by contacting the lead contact W.X..

Pathway thermodynamics and enzyme protein cost analysis

Thermodynamics and enzyme protein cost analysis were applied to assess the feasibility of a native or designed metabolic pathway as well as corresponding protein burden. Pathway feasibility was evaluated by solving a max-min driving force (MDF) problem which seek to maximize the Gibbs energy change, ΔG', of the most thermodynamically unfavorable reaction by tuning the concentrations of intermediates, which is defined as[12, 13, 14]:

$$\begin{aligned} max\ & \min(-\Delta G_1^{'}, -\Delta G_2^{'}, ..., -\Delta G_m^{'}) \\ s.t.\ & \Delta G_i^{'} = \Delta G_i^{'0} + R \cdot T \cdot \mathbf{S} \cdot \ln(\mathbf{c})\ \ (i = 1, 2, ..., m) \\ & \ln(\mathbf{c}_{\min}) \le \ln(\mathbf{c}) \le \ln(\mathbf{c}_{\max}) \end{aligned}$$

where m is the number of pathway enzymes, **c** is the vector of involved metabolite concentrations with upper bounds and lower bounds as $\mathbf{c}_{min}$ and $\mathbf{c}_{max}$, respectively, and **S** is the stoichiometric matrix of the pathway reactions.

In contrast, enzyme protein cost analysis aims to estimate the minimal protein mass required to support a unit pathway flux by solving a nonlinear optimization problem[12, 14]:

$$\begin{aligned} min\ & \Lambda = \frac{\sum_{i}^{m} (MW_i \cdot E_i)}{v_{in}} \\ s.t.\ & \ln(\mathbf{c}_{\min}) \le \ln(\mathbf{c}) \le \ln(\mathbf{c}_{\max}) \end{aligned}$$

where v_{in} denotes influx to a pathway, MW is enzyme molecular weight, and E is the expression of reaction enzyme level derived from a common modular rate law[21] and Haldane relationship[22].

The calculation was performed using a Python-based pathway analysis tool, PathParser[14]. The thermodynamic and kinetic parameters of enzymes in the WLP and the designed reductive acetyl-CoA Bi-cycle pathway (with CO_2 and formate fixation) were listed in Table S2, 3 and 4. The tandard Gibbs free energies ($\Delta G'^{m}$) were searched in eQuilibrator database[23]. Michaelis constants (K_m), catalytic rate constants (k_{cat}) and enzyme molecular weight (MW) of *C. ljungdahlii*, *M. thermoacetica*, *Acetobacterium* woodii, *Clostridium formicoaceticum*[24] and *E. coli* were preferential chosen from Brenda[25]. If no data are available, default values of 200 s^{-1}, 0.2 mM and 40 kDa were used, respectively.

During optimization, concentrations of involved metabolites were constrained to vary between 1 μM and 10mM[14].

Metabolic robustness analysis

Pathway stability was evaluated using an ensemble modeling approach combined with the continuation method[17]. First, an ensemble of models were generated with randomly sampled kinetic parameters from the feasible spaces, meanwhile subjecting to the same flux distribution of reference state[15, 16]. Then the continuation method was used to simulate the system response to enzyme expression perturbations by integrating the differential equations[14, 17]:

$$\frac{d\mathbf{c}_{SS}}{d\mathbf{E}} = -(\frac{\partial \mathbf{f}}{\partial \mathbf{c}_{SS}})^{-1} \cdot \frac{\partial \mathbf{f}}{\partial \mathbf{E}}$$

where $\mathbf{c}_{SS}$ denotes metabolite concentrations at steady state, **f** denotes the derivative of the concentrations with respect to time, and the Jacobian matrix $\frac{\partial \mathbf{f}}{\partial \mathbf{c}_{SS}}$ determines the metabolic robustness of pathway in which a system failure occurs when real part of any of the Jacobian eigenvalues pass through zero. Robustness analysis of native WLP and the designed reductive acetyl-CoA Bi-cycle pathway was also performed by PathParser [14] with an ensemble of 100 generated models.

Genome scale flux balance analysis

The synergy of reductive acetyl-CoA bi-cycle and the WLP for ethanol and acetate production under different growth mode was evaluated by flux balance analysis using the metabolic modeling package COBRApy[19]. We adapted the genome-scale metabolic model (iHN637) which consists of 785 reactions and 698 metabolites including all the major central metabolic and biosynthetic pathways in *C. ljungdahlii*[26] by adding the phosphoketolase reaction into the model. In autotrophic model, uptake of CO, CO_2 and H_2 were allowed as carbon and electron donor, whereas fructose was consumed in heterotrophic mode with CO_2 emission. Both fructose and CO were used as substrate in mixotrophic mode of *C. ljungdahlii*.

Visualization of proteomic data

Proteomic data was visualized with an online illustration tool Proteomaps which shows the quantitative composition of proteomes according to protein function[27]. Details of description and usage of the tool can be found at: https://www.proteomaps.net/index.html.

Experimental analysis

Strains, media, and chemicals

C. ljungdahlii DSM 13528 was purchased from the Leibniz Institute DSMZ (Braunschweig, Germany). The *C. ljungdahlii* ACS deficient strain OTA1 was a gift from Dr. Amy M Grunden at NC State University[28]. The YTF rich medium consisting of 10 g L^{-1} Bacto yeast extract, 16 g L^{-1} Bacto tryptone, 4 g L^{-1} NaCl, 5 g L^{-1} fructose and 0.5 g L^{-1} cysteine-HCl and the defined PETC medium were utilized for growing *C. ljungdahlii*. Cell growth was monitored at 600nm with a DU 800 spectrophotometer (Beckman-Coulter, Brea, CA). All chemical reagents used in growth studies were purchased from Sigma-Aldrich, except Bacto yeast extract and tryptone which were purchased from Becton Dickinson.

Phosphoketolase expression in *E. coli*, purification, and activity assay

The phosphoketolase (CA_C1343) gene from *C. acetobutylicum* ATCC 824 was synthesized from Genscript and cloned into plasmid pET28a. The successful transformants were confirmed by DNA sequencing. *E. coli* (DE3) containing the expression plasmid for N-terminal His6-tagged protein was grown on LB medium to an OD of 0.8 at 37°C, induced by 0.2 mM IPTG and harvested after overnight shaking at room temperature. Protein purification was performed according to a nickel-nitrilotriacetic (Ni-NTA) agarose minicolumn protocol[29]. The purified protein was run on a sodium dodecyl sulfate-polyacrylamide gel to monitor its size and purity. Phosphoketolase activity was measured using enzyme-linked assay[30]. Briefly, the assay included 50 mM Tri-HCl pH7.5, 5 mM $MgCl_2$, 5 mM K_3PO_4, 1 mM ADP, 2 mM glucose, 0.2 mM NADP, 0.5 U glucose kinase, 0.5 U glucose-6-phosphate 1-dehydrogenase, 1 mM thiamine pyrophosphate (TPP), 1U acetate kinase, 10 mM of ribose 5-phosphate, 2U ribulose 5-phosphate 3-epimerase, 2U ribose-5-phosphate isomerase and 2 µg purified phosphoketolase. The formation of NADPH was recorded at 340 nm by plate reader.

Construction of acb strains in *C. ljungdahlii*

Plasmid pMTL82151 was from Chain Biotech (Nottingham, UK) and used to generate the constructs transformed into *C. ljungdahlii*. The *C. ljungdahlii pta* promoter was amplified

from gDNA and linked with the phosphoketolase to drive expression. To construct the plasmid, pMTL82151 was linearized with SmaI and ligated with the *pta* promoter and phosphoketolase gene using Gibson assembly from New England Biolabs (Ipswich, MA). Transformation was based on previously reported protocols[31]. Briefly, cultures were grown in 40 mM DL-Threonine to mid log phase (OD 0.4-0.8), then harvested by centrifugation. Cells were washed twice with ice cold SMP buffer (270 mM sucrose, 1 mM $MgCl_2$, 7 mM sodium phosphate, pH 6), then resuspended in SMP buffer with 10% dimethyl sulfoxide (DMSO) and stored at -80°C until used for transformation. Electrotransformation was performed in a COY anaerobic chamber with Gene Pulser Xcell Bio-Rad electroporator (Hercules, CA) with the following settings: in a 1 mm cuvette, 25 µL cells were mixed with 2-5 µg of DNA, pulsed 625 kV with resistance at 600 Ω and a capacitance of 25 µF. Cells were then resuspended in 5 mL of YTF and recovered overnight at 37°C. Cells were plated in 1.5% agar YTF with thiamphenicol (Tm) at a concentration of 10 µg/mL.

Activity assay of phosphoketolase in *C. ljungdahlii*

Cells in mid log phase (OD 0.4-0.8) were harvested by centrifugation. Cell pellets were resuspended in 500 µL 50 mM histidine-HCl buffer (pH 7.0) containing 20 mM KH_2PO_4-Na_2HPO_4, 2 mM dithiothreitol, 1 mM $MgSO_4$ and 5 µg Read-Lyse lysozyme (Lucigen, Middleton, WI). Resuspended cells were added to a screwcap tube containing acid washed glass beads (Sigma-Aldrich, St. Louis, MO) and lysed using a Tissuelyser II (Qiagen, Hilden, Germany) at a frequency of 30 s^{-1} for 2 min. Cell free extract was made by spinning lyse cells at 15,000g for 3 minutes and taking the supernatant.

Phosphoketolase activity assay was adapted from previously reported protocols[29, 32]. Briefly, cell free extracts of the wild-type and transformed phosphoketolase strain were added to buffer containing 25 mM xylulose 5-phosphate to generate acetyl-P, which was then converted to acetate by adding 1 µl of 1 M $MgCl_2$, 1 µl of 30 mM ADP, and 0.2 U of acetate kinase to 75 µl of the assay mixture and incubating at 30°C for 30 minutes. The acetate was then determined enzymatically with the Acetic Acid Assay Kit (Megazyme, Bray, Ireland), using an assay mixture without xylulose 5-phosphate as a control.

Proteome measurement and analysis

The proteomic analysis of wild type and acb strains were conducted following the same method in our previous report[14]. 10 µg of trypsin digested peptides from each sample were loaded onto a C18 capillary column coupled to a Thermo LTQ Orbitrap mass spectrometry (Thermo-Scientific, Rockford, IL). The peptide identity was analyzed at the resolution of 30,000. Dynamic exclusion was enabled in this case with the set up of repeat count of 1, repeat duration of 30 seconds, and exclusion duration of 90 seconds. The peptide identify was obtained by searching the tandem MS spectra using Patternlab for Proteomics[33].

Analysis of *C. ljungdahlii* strains grown under heterotrophic, mixotrophic and autotrophic conditions

C. ljungdahlii was first grown in liquid YTF medium, then centrifuged (Beckman-Coulter, Brea, CA) at 4000g for 15 min. The pellet was transferred into PETC medium with 5 g L^{-1} fructose and grown on a MaxQ 5000 shaker (Thermo Fisher Scientific, Waltham, MA) at 37°C. Cells in mid log phase (OD 0.4-0.8) were harvested again by centrifugation at 4000g for 15 min, and the pellet was transferred to Duran Pressure Plus laboratory bottles (DWK Life Sciences, Mainz, Germany) containing PETC media with 5 g L^{-1} fructose for heterotrophic and mixotrophic growth or no fructose for autotrophic growth.

The bottles for autotrophic and mixotrophic growth were degassed with a 4:1 v/v blend of CO/CO_2 then pressurized to 2 psi. The cultures were grown at 37°C, 220rpm on the MaxQ 5000 shaker. Cell growth was monitored every 24 or 48 hours. Headspace pressure was measured with an DG25 Digital Pressure Gauge (Ashcroft, Stratford, CT), and metabolites including acetate and ethanol were analyzed by an Agilent 1200 high-pressure liquid chromatography (Santa Clara, CA) with an Aminex HPX-87H column using 4 mM H_2SO_4 as the eluent. Liquid samples were filtered prior to analysis.

^{13}C-labeling experiment and metabolite measurement by GC-MS

20 mM [U-$^{13}C_2$] acetate was fed to PETC media for tracking modules' activities in autotrophic and heterotrophic cultures. Autotrophic *C. ljungdahlii* cells were grown in sealed bottles with a 4:1 v/v blend of CO/CO_2 in the headspace. Heterotrophic cultures were supplied with no gas substrates but 5 g/L fructose in the media. Cells in mid log phase (OD 0.4-0.8) were harvested and pretreated as described previously[34]. Labeling

patterns of proteinogenic amino acids from cell mass were then analyzed by Gas Chromatograph-Mass Spectrometry (GC-MS) as previously reported[35, 36].

Acknowledgments

We acknowledge Dr. Amy M. Grunden at North Carolina State University for providing an acetyl-CoA synthase deficient *C. ljungdahlii* OTA1. **Funding**: This work was authored in part by Alliance for Sustainable Energy, LLC, the manager, and operator of the National Renewable Energy Laboratory for the U.S. Department of Energy (DOE) under Contract No. DE-AC36-08GO28308. This work is supported by a Laboratory Directed Research and Development (LDRD) project at the National Renewable Energy Laboratory to W.X. and partially by Shell International Exploration and Production Inc. to P.M. and W.X. **Author contributions**: W.X. projects conception. C.W., W.X. designed and performed all computational biology analysis. J.L. designed and performed genetic engineering on *C. ljungdahlii*. J.L., C.U., X.G., J.H. and W.X. performed experiments including cell culture, enzyme assay, gas fermentation and product measurement. C.W., C.U., X.G. and W.X. designed and performed ^{13}C-labeling experiments and GC-MS analysis. S.S., X.W., C.W., and W.X. generated and analyzed proteomics data. C.W. and W.X. wrote the manuscript with input from all co-authors and revisions from K.J.C., P.M., N.T. and D.P. **Competing interests**: Authors declare no competing interests**.**

References

1. Sun X, Atiyeh HK, Huhnke RL, Tanner RS. Syngas fermentation process development for production of biofuels and chemicals: A review. *Bioresource Technology Reports* **7**, 100279 (2019).

2. Jones SW*, et al.* CO2 fixation by anaerobic non-photosynthetic mixotrophy for improved carbon conversion. *Nat Commun* **7**, 12800 (2016).

3. Munasinghe PC, Khanal SK. Syngas fermentation to biofuel: Evaluation of carbon monoxide mass transfer coefficient (kLa) in different reactor configurations. *Biotechnology Progress* **26**, 1616-1621 (2010).

4. Can M, Armstrong FA, Ragsdale SW. Structure, Function, and Mechanism of the Nickel Metalloenzymes. *Chemical Reviews* **114**, 4149-4174 (2014).

5. Leaphart AB, Trent Spencer H, Lovell CR. Site-directed mutagenesis of a potential catalytic and formyl phosphate binding site and substrate inhibition of N10-formyltetrahydrofolate synthetase. *Archives of Biochemistry and Biophysics* **408**, 137-143 (2002).

6. Bogorad IW, Lin T-S, Liao JC. Synthetic non-oxidative glycolysis enables complete carbon conservation. *Nature* **502**, 693-697 (2013).

7. Köpke M*, et al.* Clostridium ljungdahlii represents a microbial production platform based on syngas. *Proceedings of the National Academy of Sciences* **107**, 13087-13092 (2010).

8. Xiong W*, et al.* CO2-fixing one-carbon metabolism in a cellulose-degrading bacterium Clostridium thermocellum. *Proceedings of the National Academy of Sciences* **113**, 13180-13185 (2016).

9. Furdui C, Ragsdale SW. The Role of Pyruvate Ferredoxin Oxidoreductase in Pyruvate Synthesis during Autotrophic Growth by the Wood-Ljungdahl Pathway. *Journal of Biological Chemistry* **275**, 28494-28499 (2000).

10. Tremblay P-L, Zhang T, Dar SA, Leang C, Lovley DR. The Rnf Complex of Clostridium ljungdahlii Is a Proton-Translocating Ferredoxin:NAD+ Oxidoreductase Essential for Autotrophic Growth. *mBio* **4**, (2013).

11. Liew F, Henstra AM, Kpke M, Winzer K, Simpson SD, Minton NP. Metabolic engineering of Clostridium autoethanogenum for selective alcohol production. *Metab Eng* **40**, 104-114 (2017).

12. Flamholz A, Noor E, Bar-Even A, Liebermeister W, Milo R. Glycolytic strategy as a tradeoff between energy yield and protein cost. *Proceedings of the National Academy of Sciences* **110**, 10039-10044 (2013).

13. Noor E, Bar-Even A, Flamholz A, Reznik E, Liebermeister W, Milo R. Pathway thermodynamics highlights kinetic obstacles in central metabolism. *PLoS Comput Biol* **10**, e1003483 (2014).

14. Wu C*, et al.* A generalized computational framework to streamline thermodynamics and kinetics analysis of metabolic pathways. *Metab Eng* **57**, 140-150 (2020).

15. Tran LM, Rizk ML, Liao JC. Ensemble modeling of metabolic networks. *Biophys J* **95**, 5606-5617 (2008).

16. Tan Y, Rivera JG, Contador CA, Asenjo JA, Liao JC. Reducing the allowable kinetic space by constructing ensemble of dynamic models with the same steady-state flux. *Metab Eng* **13**, 60-75 (2011).

17. Lee Y, Lafontaine Rivera JG, Liao JC. Ensemble Modeling for Robustness Analysis in engineering non-native metabolic pathways. *Metab Eng* **25**, 63-71 (2014).

18. Orth JD, Thiele I, Palsson BØ. What is flux balance analysis? *Nature biotechnology* **28**, 245-248 (2010).

19. Ebrahim A, Lerman JA, Palsson BO, Hyduke DR. COBRApy: COnstraints-Based Reconstruction and Analysis for Python. *BMC Syst Biol* **7**, 74 (2013).

20. Könneke M*, et al.* Ammonia-oxidizing archaea use the most energy-efficient aerobic pathway for CO₂ fixation. *Proceedings of the National Academy of Sciences* **111**, 8239-8244 (2014).

21. Liebermeister W, Uhlendorf J, Klipp E. Modular rate laws for enzymatic reactions: thermodynamics, elasticities and implementation. *Bioinformatics* **26**, 1528-1534 (2010).

22. Alberty RA. Relations between biochemical thermodynamics and biochemical kinetics. *Biophysical Chemistry* **124**, 11-17 (2006).

23. Flamholz A, Noor E, Bar-Even A, Milo R. eQuilibrator--the biochemical thermodynamics calculator. *Nucleic Acids Res* **40**, D770-775 (2012).

24. Ragsdale SW, Pierce E. Acetogenesis and the Wood-Ljungdahl pathway of CO(2) fixation. *Biochim Biophys Acta* **1784**, 1873-1898 (2008).

25. Jeske L, Placzek S, Schomburg I, Chang A, Schomburg D. BRENDA in 2019: a European ELIXIR core data resource. *Nucleic Acids Res* **47**, D542-D549 (2019).

26. Nagarajan H*, et al.* Characterizing acetogenic metabolism using a genome-scale metabolic reconstruction of Clostridium ljungdahlii. *Microb Cell Fact* **12**, 118 (2013).

27. Liebermeister W, Noor E, Flamholz A, Davidi D, Bernhardt J, Milo R. Visual account of protein investment in cellular functions. *Proc Natl Acad Sci U S A* **111**, 8488-8493 (2014).

28. Whitham JM*, et al.* Characterization of Clostridium ljungdahlii OTA1: a non-autotrophic hyper ethanol-producing strain. *Appl Microbiol Biotechnol* **101**, 1615-1630 (2017).

29. Liu L*, et al.* Phosphoketolase pathway for xylose catabolism in Clostridium acetobutylicum revealed by 13C metabolic flux analysis. *J Bacteriol* **194**, 5413-5422 (2012).

30. Bogorad IW, Lin TS, Liao JC. Synthetic non-oxidative glycolysis enables complete carbon conservation. *Nature* **502**, 693-697 (2013).

31. Leang C, Ueki T, Nevin KP, Lovley DR. A genetic system for Clostridium ljungdahlii: a chassis for autotrophic production of biocommodities and a model homoacetogen. *Appl Environ Microbiol* **79**, 1102-1109 (2013).

32. Sonderegger M, Schumperli M, Sauer U. Metabolic engineering of a phosphoketolase pathway for pentose catabolism in Saccharomyces cerevisiae. *Appl Environ Microbiol* **70**, 2892-2897 (2004).

33. Carvalho PC*, et al.* Integrated analysis of shotgun proteomic data with PatternLab for proteomics 4.0. *Nat Protoc* **11**, 102-117 (2016).

34. Xiong W*, et al.* CO2-fixing one-carbon metabolism in a cellulose-degrading bacterium Clostridium thermocellum. *Proc Natl Acad Sci U S A* **113**, 13180-13185 (2016).

35. Wu C, Chen CH, Lo J, Michener W, Maness P, Xiong W. EMUlator: An Elementary Metabolite Unit (EMU) Based Isotope Simulator Enabled by Adjacency Matrix. *Front Microbiol* **10**, 922 (2019).

36. Xiong W*, et al.* Isotope-Assisted Metabolite Analysis Sheds Light on Central Carbon Metabolism of a Model Cellulolytic Bacterium Clostridium thermocellum. *Front Microbiol* **9**, 1947 (2018).

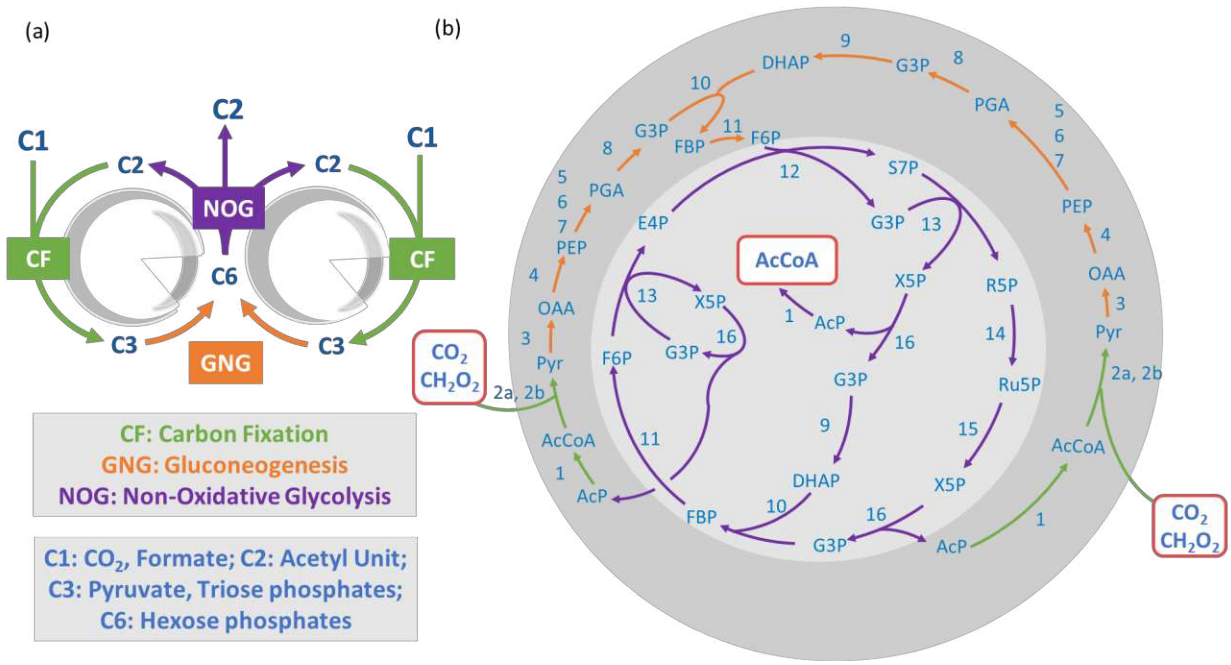

Figure 1. Reductive acetyl-CoA bi-cycle for one-carbon fixation. The schematic of the bi-cyclic pathway is shown in (a), and the detailed enzymatic reactions are shown in (b). Net stoichiometry of the designed pathway is: C1 + C1 = C2. The energetic driving force for the pathway can be from CO, H_2 and extracellular electrons. Enzymatic reactions:1. Phosphotransacetylase, 2a. Pyruvate:ferredoxin oxidoreductase (if C1= CO_2), 2b. Pyruvate formate lyase (if C1= formate), 3. Pyruvate carboxylase, 4. Phosphoenolpyruvate carboxykinase, 5. Endolase, 6. Phosphoglycerate mutase, 7. Phosphoglycerate kinase, 8. Glyceraldehyde-3-phosphate dehydrogenase, 9. Triose phosphate isomerase, 10. Fructose 1,6-bisphosphate aldolase, 11. Fructose 1,6-bisphosphatase, 12. Transaldolase, 13. Transketolase, 14. Ribose-5-phosphate isomerase, 15. Ribulose-5-phosphate epimerase, 16. Phosphoketolase. Metabolite abbreviations: AcP, Acetyl phosphate; AcCoA, Acetyl Coenzyme A; Pyr, Pyruvate; OAA, Oxaloacetate; PEP, Phosphoenolpyruvate; PGA, Phosphoglycerate; G3P, Glyceraldehyde-3-phosphate; DHAP, Dihydroxyacetone phosphate; FBP, Fructose bisphosphate; F6P, Fructose 6-phosphate; E4P, Erythrose 4-phosphate; S7P, Sedoheptulose 7-phosphate; R5P, Ribose 5-phosphate; X5P, Xylulose 5-phosphate; Ru5P, Ribulose 5-phosphate.

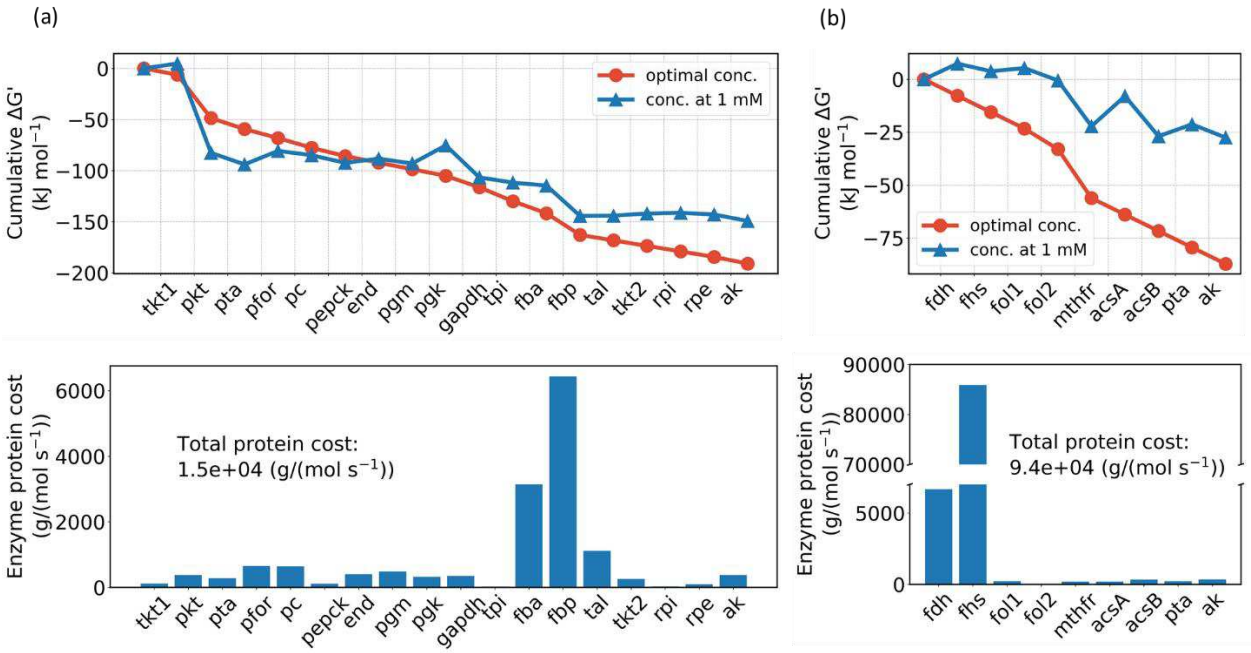

Figure 2. Thermodynamics and enzyme protein cost analysis of the reductive acetyl-CoA bi-cycle (a) and the Wood-Ljungdahl pathway (b). Thermodynamic driving force of pathway is presented as the cumulative sum of reaction Gibbs energies, ΔG'. Blue line denotes standard Gibbs energies with all metabolite concentrations fixed at 1 mM, and red line denotes Gibbs energies when the minimal ΔG′ is optimized with metabolite concentrations constrained to range from 1 μM to 10 mM. Enzyme protein costs are estimated by optimizing the total enzyme mass to support unit pathway flux with metabolite concentrations constrained to range from 1 μM to 10 mM. Enzyme abbreviations: acsA, Carbon monoxide dehydrogenase; acsB, CO-methylating acetyl-CoA synthase; ak, Acetate kinase; end, Endolase; fba, Fructose-1,6-bisphosphate aldolase; fbp, Fructose-1,6-bisphosphatase; fdh, Formate dehydrogenase; fhs, Formyltetrahydrofolate synthetase; fol1, Methenyltetrahydrofolate cyclohydrolase; fol2, Methylenetetrahydrofolate dehydrogenase; gapdh, Glyceraldehyde-3-phosphate dehydrogenase; mthfr, Methylenetetrahydrofolate reductase; pc, Pyruvate carboxylase ; pepck, Phosphoenolpyruvate carboxykinase; pfor, Pyruvate:ferredoxin oxidoreductase; pgk, Phosphoglycerate kinase; pgm, Phosphoglycerate mutase; pkt, Phosphoketolase; pta, Phosphotransacetylase; rpe, Ribulose-5-phosphate epimerase; rpi, Ribose-5-phosphate isomerase; tal, Transaldolase; tkt, Transketolase; tpi, Triose phosphate isomerase. Tkt involved in reactions with different reactants was marked with numbers. Thermodynamics and enzyme protein cost analysis of the reductive acetyl-CoA bi-cycle for formate fixation by pyruvate formate lyase is shown in Fig.S1.

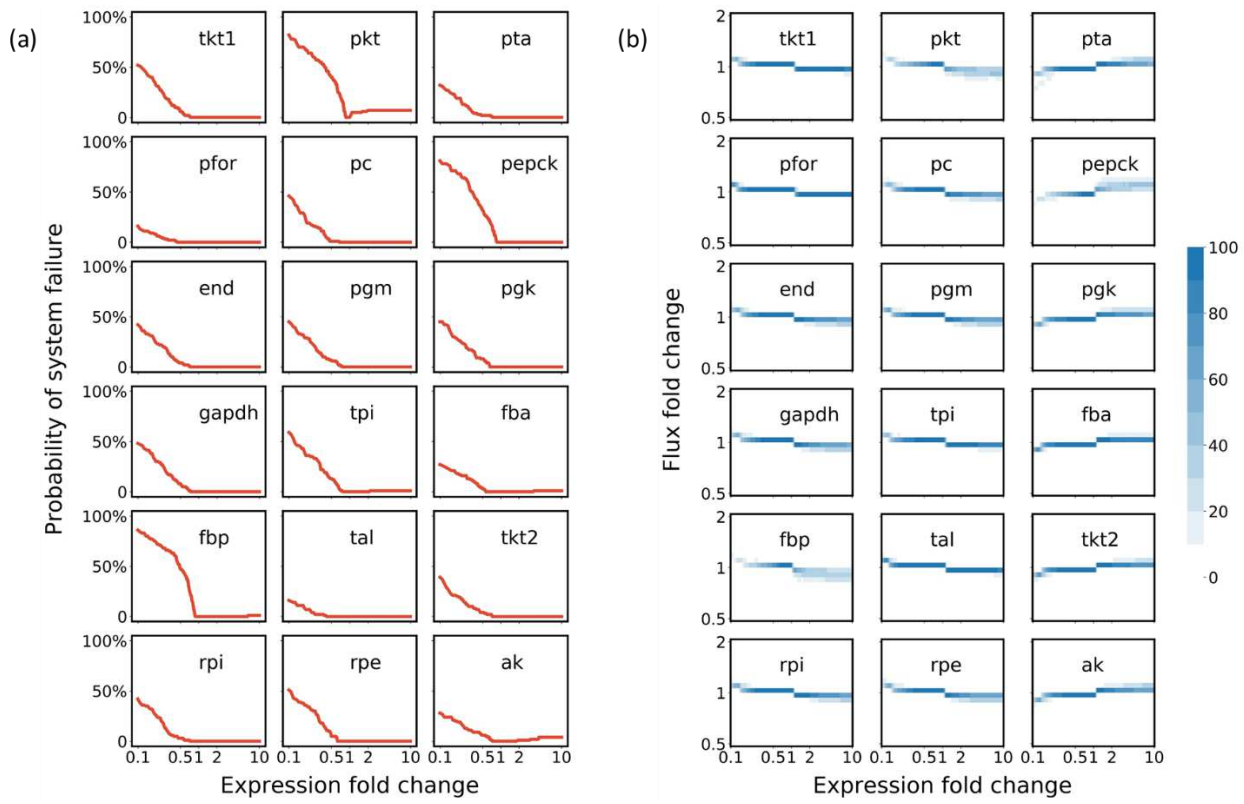

Figure 3. Pathway stability (a) and flux change (b) in response to enzyme level perturbations in the reductive acetyl- CoA Bi-cycle. Pathway stability is represented by the probability of system failure at varied fold change of enzyme expression levels over reference state. A pathway is considered as entering system failure when any intermediate is depleted or over accumulated over time, and the probability of system failure is calculated as counts in an ensemble of 100 models. The color in flux change heatmap indicates the number of models of corresponding flux fold change at some enzyme expression level. Pathway stability and flux change analysis of the reductive acetyl-CoA Bi-cycle for formate fixation by pyruvate formate lyase is shown in Fig.S2.

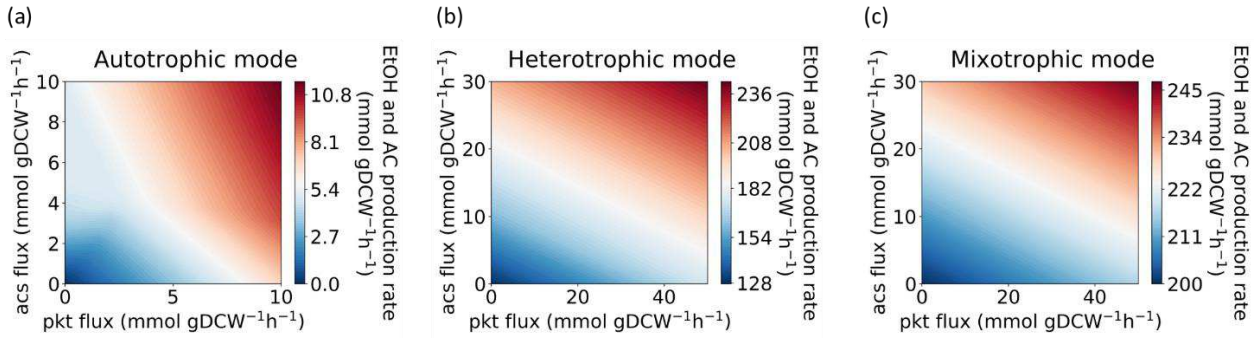

Figure 4. Contour profiling of C2 metabolites productivity as a function of the WLP and the reductive acetyl-CoA bi-cycle activity under autotrophic (a), heterotrophic (b) and mixotrophic (c) growth modes. X axis denotes the activity of acetyl-CoA bi-cycle represented by phosphoketolase (pkt) flux. Y axis denotes acetyl-CoA synthase (acs) flux as a proxy of the WLP. The contour was profiled by adapting a flux balance mode of *C. ljungdahlii*[26] with the production rate of ethanol and acetate as the objective function.

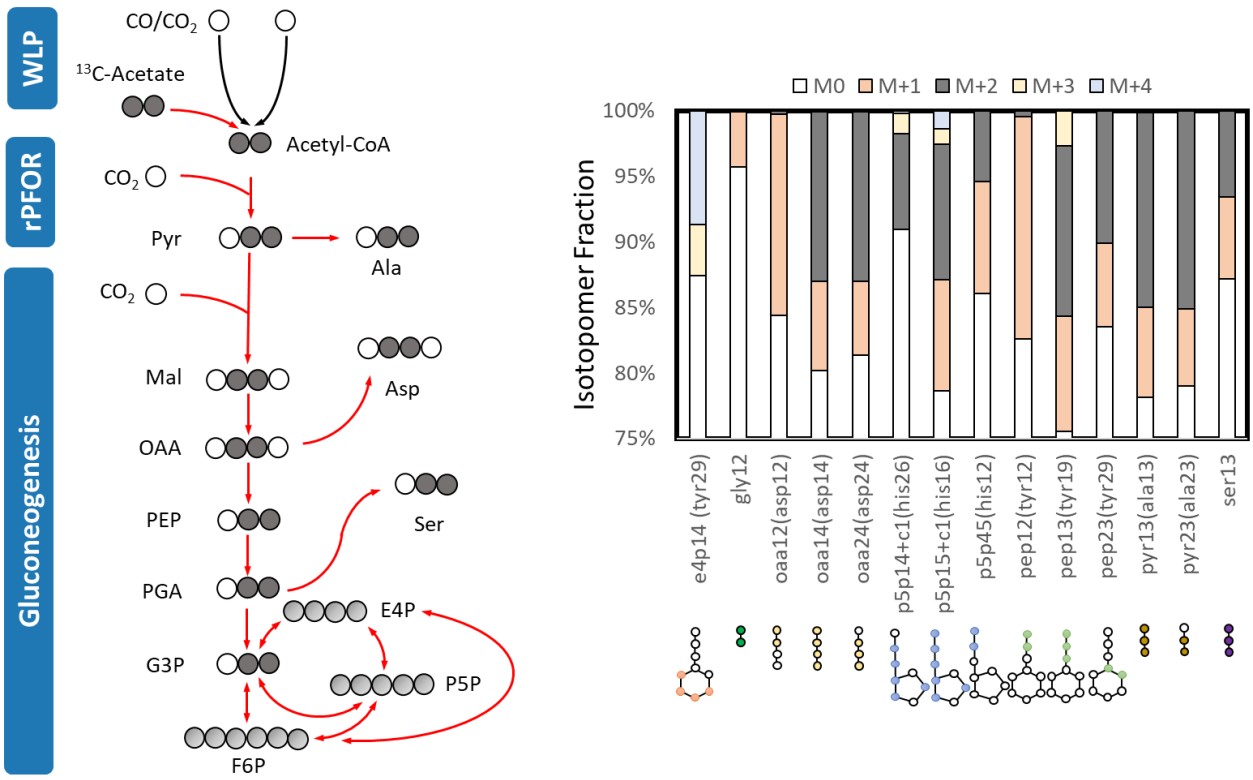

Figure 5. Functionality of carbon fixation and gluconeogenesis modules proved by labeling experiment using [U-$^{13}C_2$] acetate. Red arrows on the left denote active reactions verified by the formation of labeled downstream metabolites. Isotopomer fraction of measurable metabolite fragments are illustrated on the right. M0 denotes fraction of fragments with all ^{12}C carbon atoms, and M+i denotes fraction of fragments with i carbons labeled with ^{13}C. In right panel, labeled metabolites are presented as "precursor fragment (amino acid fragment)", and contributing carbon atoms from the precursor are colored.

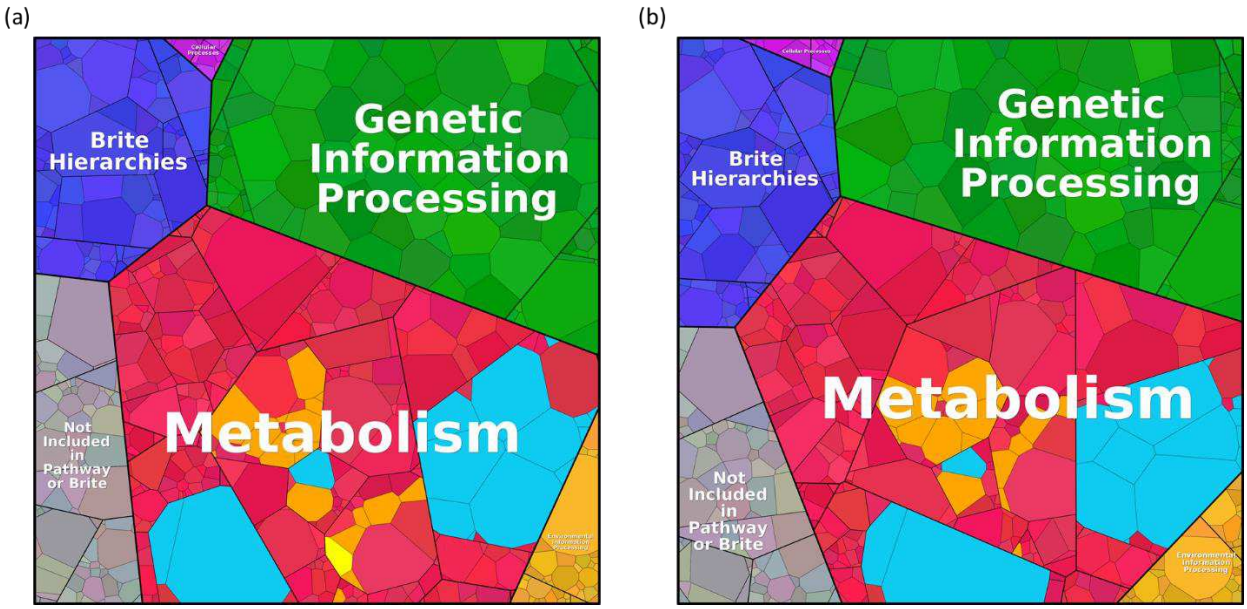

Figure 6. Pathway enzyme allocation in the proteome of *C. ljungdahlii* acb strain (a) and wild type (wt) strain (b) grown on CO and CO_2. Pathway enzymes for carbon fixation are under the Metabolism category. Every tile (small polygon) represents one type of protein. Tile sizes represent the mass fractions of proteins. The enzymes in the Wood-Ljungdahl pathway are shown in cyan and enzymes in the reductive acetyl-CoA bi-cycle are shown in ocher. Engineered phosphoketolase are shown in bright yellow. See Fig.S5 for detailed proteomaps.

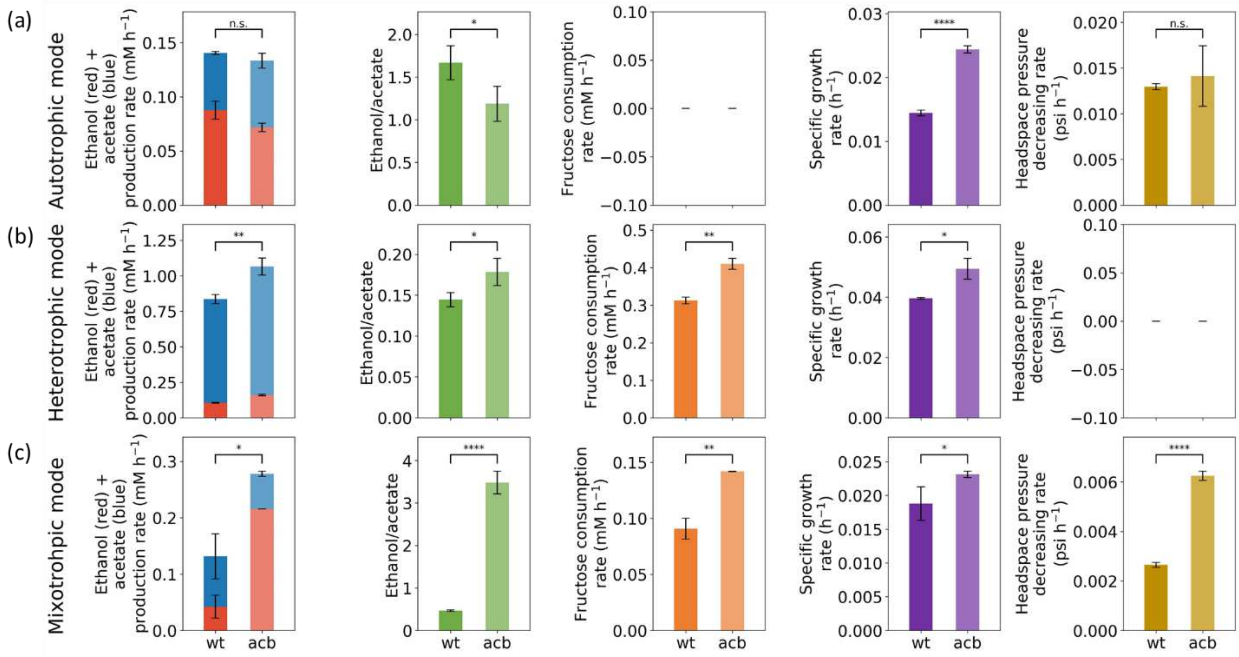

Figure 7. Growth and productivities of the strain carrying acetyl-CoA bi-cycle (acb) under autotrophic (a), heterotrophic (b) and mixotrophic (c) modes in comparison with wt *C. ljungdahlii*. Error bars represent standard deviations from biological triplicates. Student's t-test was performed to compare the difference of each specie in three replicates. '*' denotes pvalue < 0.05, '**' denotes pvalue < 0.005, '****' denotes pvalue < 0.00005 and 'n.s.' denotes no significance.

Figures

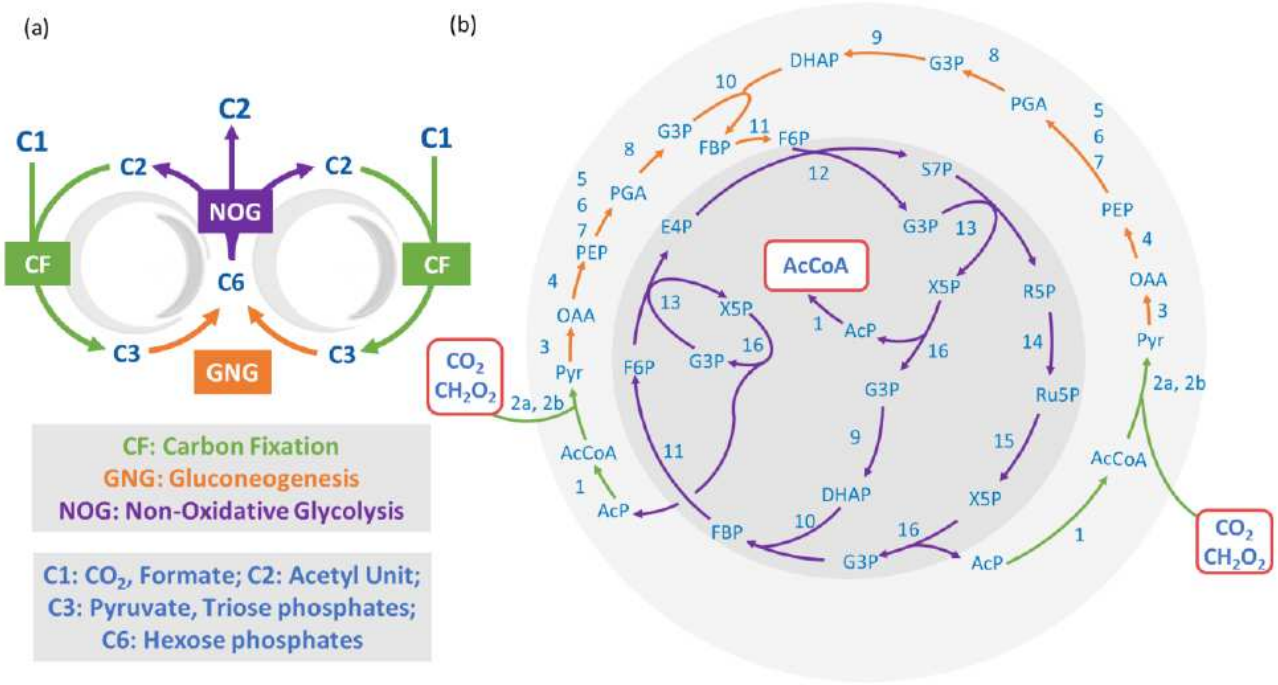

Figure 1

Reductive acetyl-CoA bi-cycle for one-carbon fixation. The schematic of the bi-cyclic pathway is shown in (a), and the detailed enzymatic reactions are shown in (b). Net stoichiometry of the designed pathway is: C1 + C1 = C2. The energetic driving force for the pathway can be from CO, H2 and extracellular electrons. Enzymatic reactions:1. Phosphotransacetylase, 2a. Pyruvate:ferredoxin oxidoreductase (if C1= CO2), 2b. Pyruvate formate lyase (if C1= formate), 3. Pyruvate carboxylase, 4. Phosphoenolpyruvate carboxykinase, 5. Endolase, 6. Phosphoglycerate mutase, 7. Phosphoglycerate kinase, 8. Glyceraldehyde-3-phosphate dehydrogenase, 9. Triose phosphate isomerase, 10. Fructose 1,6-bisphosphate aldolase, 11. Fructose 1,6-bisphosphatase, 12. Transaldolase, 13. Transketolase, 14. Ribose-5-phosphate isomerase, 15. Ribulose-5-phosphate epimerase, 16. Phosphoketolase. Metabolite abbreviations: AcP, Acetyl phosphate; AcCoA, Acetyl Coenzyme A; Pyr, Pyruvate; OAA, Oxaloacetate; PEP, Phosphoenolpyruvate; PGA, Phosphoglycerate; G3P, Glyceraldehyde-3-phosphate; DHAP, Dihydroxyacetone phosphate; FBP, Fructose bisphosphate; F6P, Fructose 6-phosphate; E4P, Erythrose 4-phosphate; S7P, Sedoheptulose 7-phosphate; R5P, Ribose 5-phosphate; X5P, Xylulose 5-phosphate; Ru5P, Ribulose 5-phosphate.

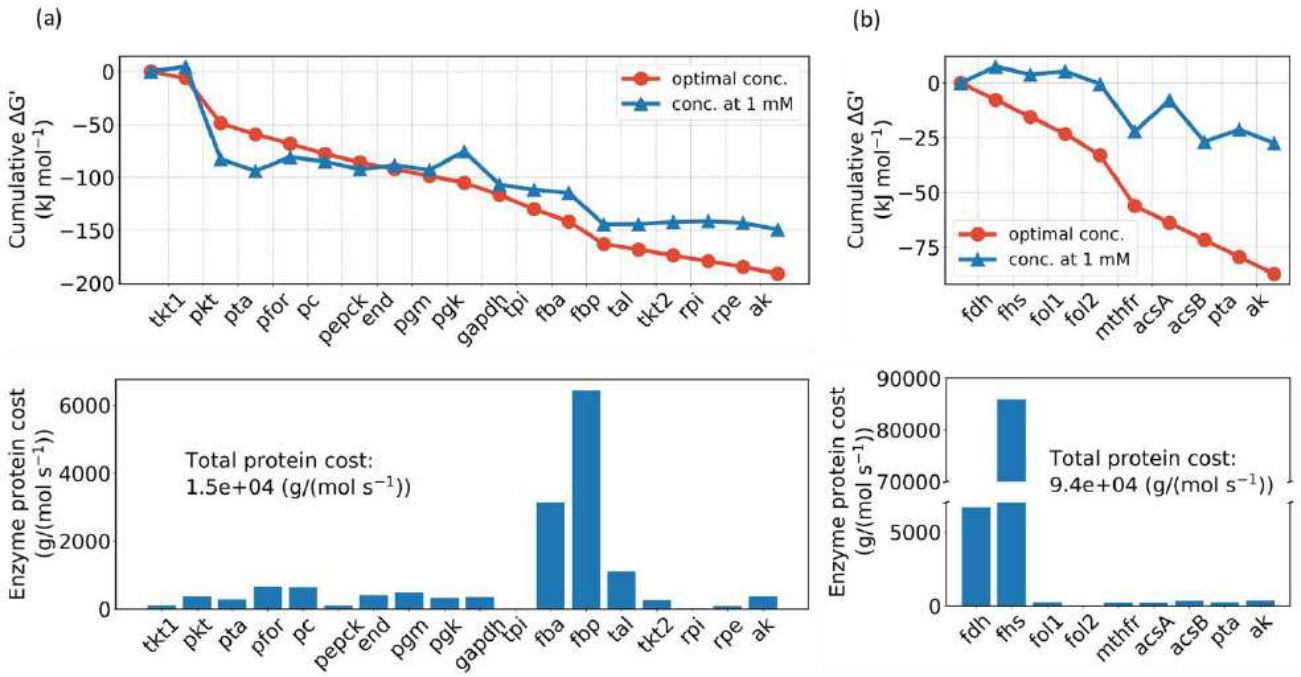

Figure 2

Thermodynamics and enzyme protein cost analysis of the reductive acetyl-CoA bi-cycle (a) and the Wood-Ljungdahl pathway (b). Thermodynamic driving force of pathway is presented as the cumulative sum of reaction Gibbs energies, ΔG'. Blue line denotes standard Gibbs energies with all metabolite concentrations fixed at 1 mM, and red line denotes Gibbs energies when the minimal ΔG' is optimized with metabolite concentrations constrained to range from 1 μM to 10 mM. Enzyme protein costs are estimated by optimizing the total enzyme mass to support unit pathway flux with metabolite concentrations constrained to range from 1 μM to 10 mM. Enzyme abbreviations: acsA, Carbon monoxide dehydrogenase; acsB, CO-methylating acetyl-CoA synthase; ak, Acetate kinase; end, Endolase; fba, Fructose-1,6-bisphosphate aldolase; fbp, Fructose-1,6-bisphosphatase; fdh, Formate dehydrogenase; fhs, Formyltetrahydrofolate synthetase; fol1, Methenyltetrahydrofolate cyclohydrolase; fol2, Methylenetetrahydrofolate dehydrogenase; gapdh, Glyceraldehyde-3-phosphate dehydrogenase; mthfr, Methylenetetrahydrofolate reductase; pc, Pyruvate carboxylase ; pepck, Phosphoenolpyruvate carboxykinase; pfor, Pyruvate:ferredoxin oxidoreductase; pgk, Phosphoglycerate kinase; pgm, Phosphoglycerate mutase; pkt, Phosphoketolase; pta, Phosphotransacetylase; rpe, Ribulose-5-phosphate epimerase; rpi, Ribose-5-phosphate isomerase; tal, Transaldolase; tkt, Transketolase; tpi, Triose phosphate isomerase. Tkt involved in reactions with different reactants was marked with numbers. Thermodynamics and enzyme protein cost analysis of the reductive acetyl-CoA bi-cycle for formate fixation by pyruvate formate lyase is shown in Fig.S1.

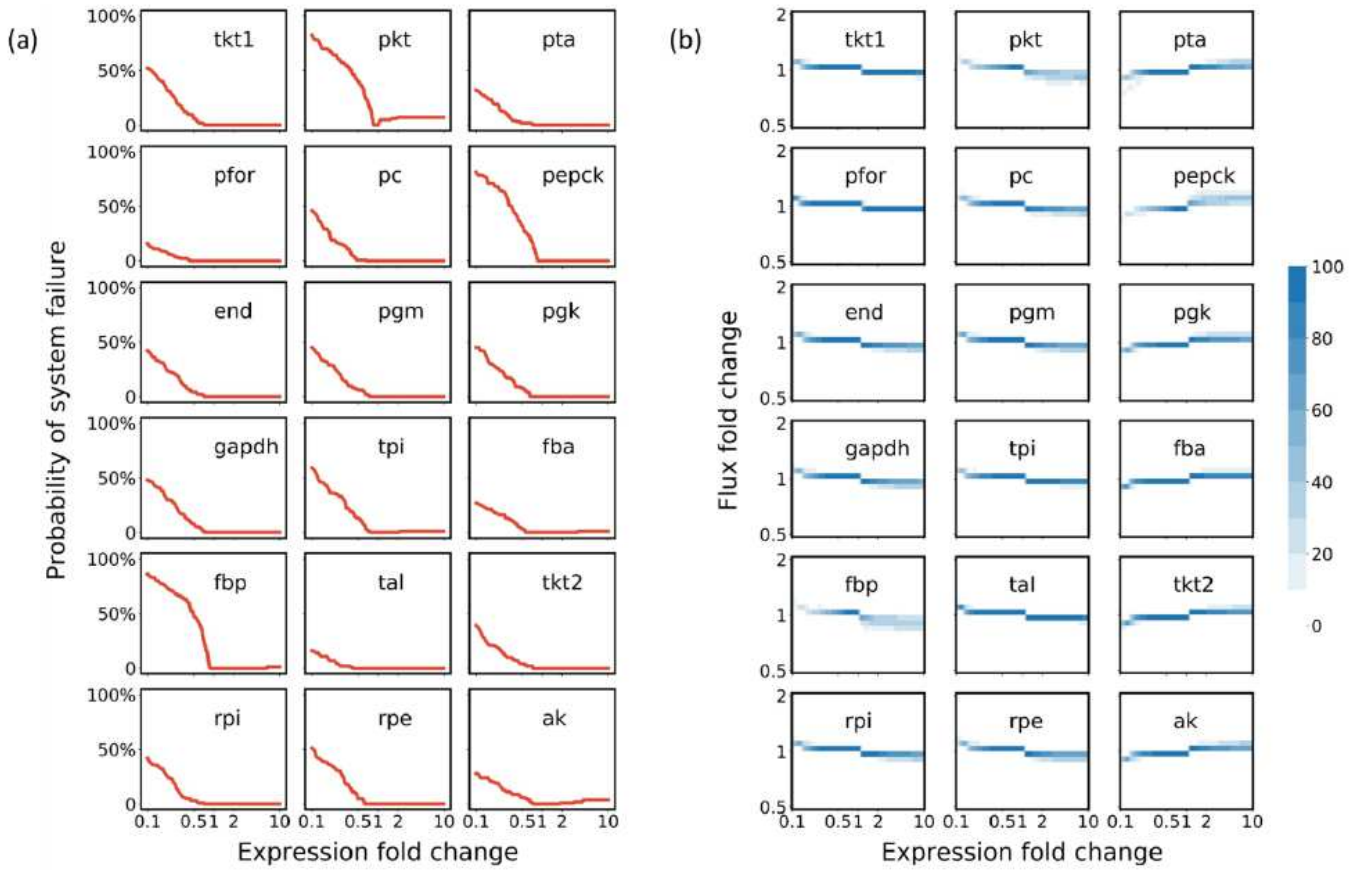

Figure 3

Pathway stability (a) and flux change (b) in response to enzyme level perturbations in the reductive acetyl- CoA Bi-cycle. Pathway stability is represented by the probability of system failure at varied fold change of enzyme expression levels over reference state. A pathway is considered as entering system failure when any intermediate is depleted or over accumulated over time, and the probability of system failure is calculated as counts in an ensemble of 100 models. The color in flux change heatmap indicates the number of models of corresponding flux fold change at some enzyme expression level. Pathway stability and flux change analysis of the reductive acetyl-CoA Bi-cycle for formate fixation by pyruvate formate lyase is shown in Fig.S2.

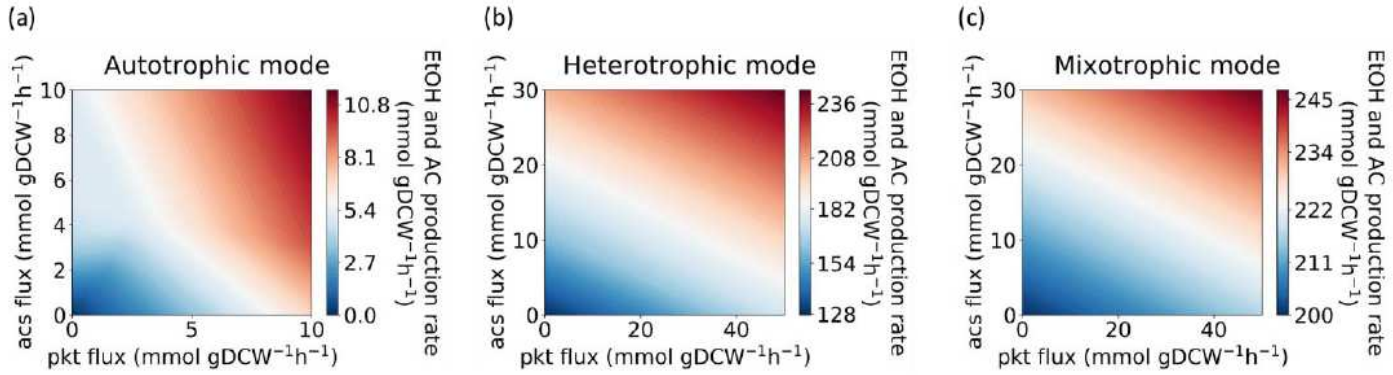

Figure 4

Contour profiling of C2 metabolites productivity as a function of the WLP and the reductive acetyl-CoA bi-cycle activity under autotrophic (a), heterotrophic (b) and mixotrophic (c) growth modes. X axis denotes the activity of acetyl-CoA bi-cycle represented by phosphoketolase (pkt) flux. Y axis denotes acetyl-CoA synthase (acs) flux as a proxy of the WLP. The contour was profiled by adapting a flux balance mode of C. ljungdahlii26 with the production rate of ethanol and acetate as the objective function.

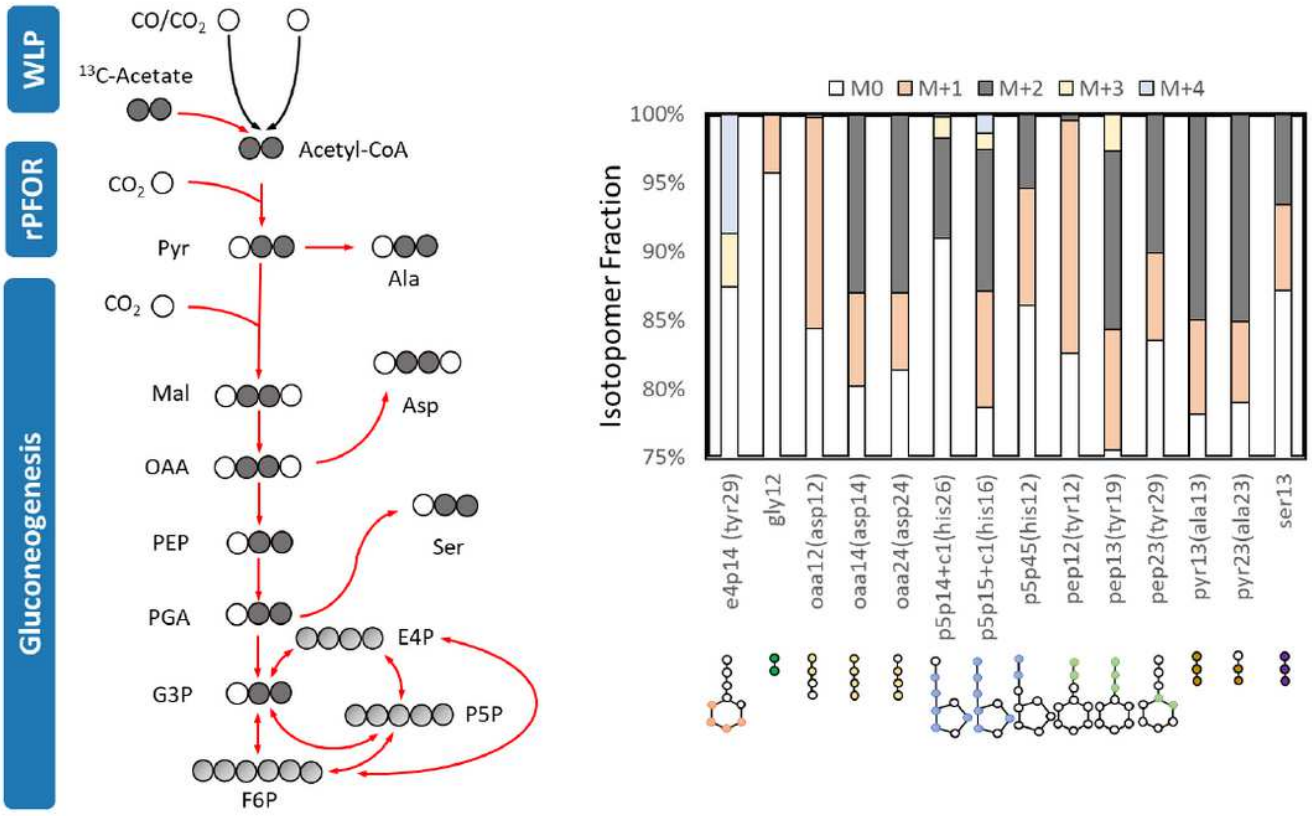

Figure 5

Functionality of carbon fixation and gluconeogenesis modules proved by labeling experiment using [U-13C2] acetate. Red arrows on the left denote active reactions verified by the formation of labeled downstream metabolites. Isotopomer fraction of measurable metabolite fragments are illustrated on the right. M0 denotes fraction of fragments with all 12C carbon atoms, and M+i denotes fraction of fragments with i carbons labeled with13C. In right panel, labeled metabolites are presented as “precursor fragment (amino acid fragment)”, and contributing carbon atoms from the precursor are colored.

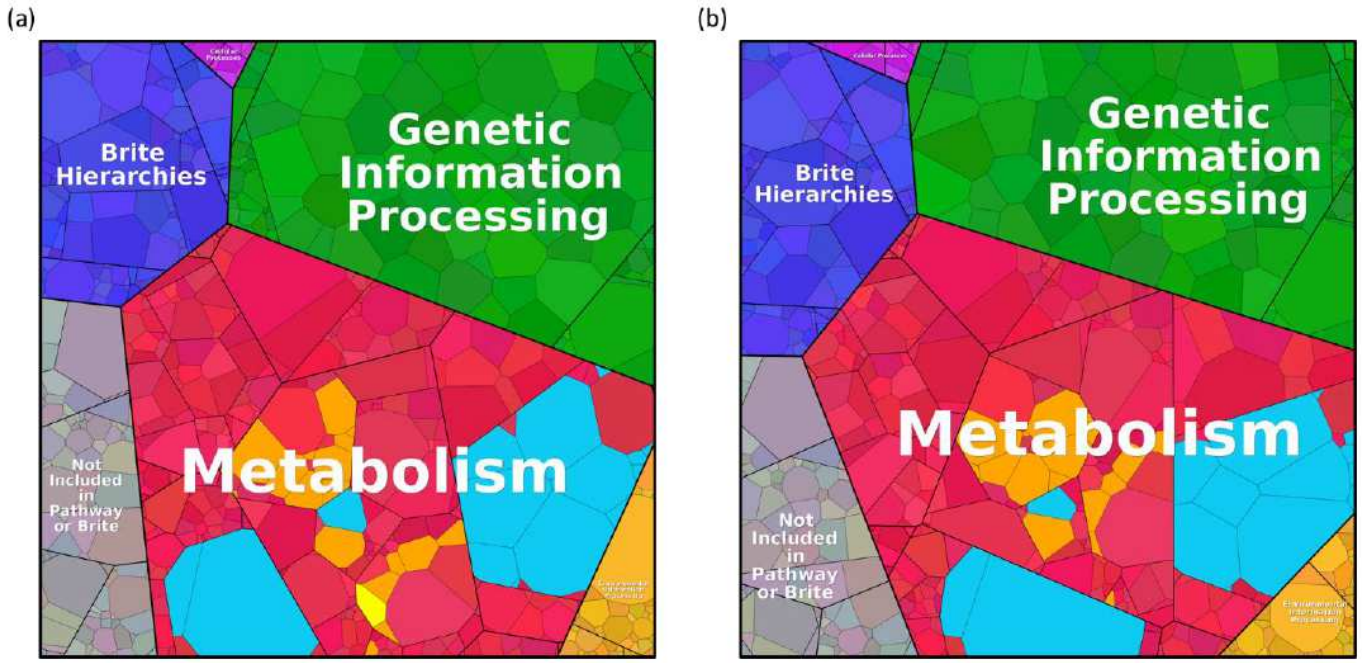

Figure 6

Pathway enzyme allocation in the proteome of C. ljungdahlii acb strain (a) and wild type (wt) strain (b) grown on CO and CO2. Pathway enzymes for carbon fixation are under the Metabolism category. Every tile (small polygon) represents one type of protein. Tile sizes represent the mass fractions of proteins. The enzymes in the Wood-Ljungdahl pathway are shown in cyan and enzymes in the reductive acetyl-CoA bi-cycle are shown in ocher. Engineered phosphoketolase are shown in bright yellow. See Fig.S5 for detailed proteomaps.

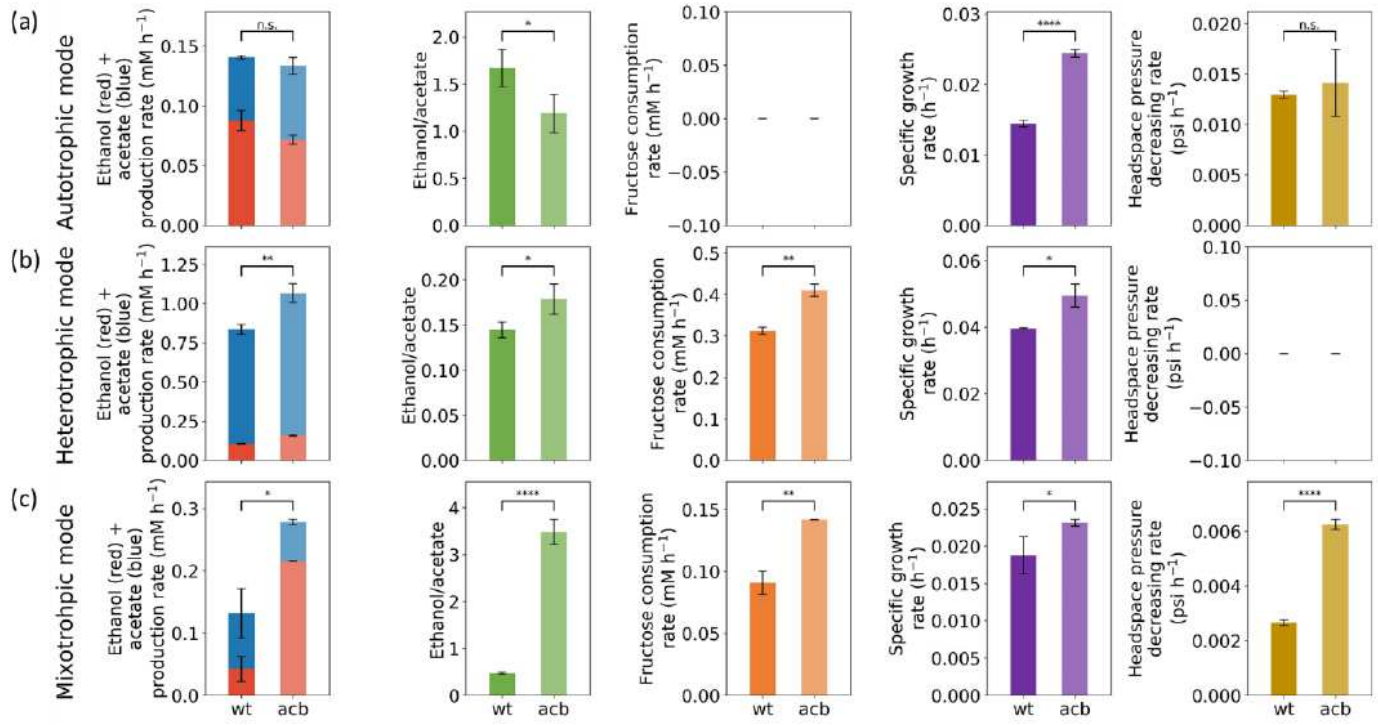

Figure 7

Growth and productivities of the strain carrying acetyl-CoA bi-cycle (acb) under autotrophic (a), heterotrophic (b) and mixotrophic (c) modes in comparison with wt C. ljungdahlii. Error bars represent standard deviations from biological triplicates. Student's t-test was performed to compare the difference of each specie in three replicates. '*' denotes pvalue < 0.05, '**' denotes pvalue < 0.005, '****' denotes pvalue < 0.00005 and 'n.s.' denotes no significance.

Supplementary Files

This is a list of supplementary files associated with this preprint. Click to download.

- SupplementaryInformation.docx